

# Dynamics of the unitary Bose gas near a narrow Feshbach resonance: universal coherent atom-molecule oscillations

Ke Wang,<sup>1,2</sup> Zhendong Zhang,<sup>3</sup> Shu Nagata,<sup>1</sup> Zhiqiang Wang,<sup>1,4,5,6</sup> and K. Levin<sup>1</sup>

<sup>1</sup>Department of Physics and James Franck Institute, University of Chicago, Chicago, Illinois 60637, USA

<sup>2</sup>Kadanoff Center for Theoretical Physics, University of Chicago, Chicago, Illinois 60637, USA

<sup>3</sup>E. L. Ginzton Laboratory and Department of Applied Physics, Stanford University, Stanford, CA 94305, USA

<sup>4</sup>Hefei National Research Center for Physical Sciences at the Microscale and School of Physical Sciences, University of Science and Technology of China, Hefei, Anhui 230026, China

<sup>5</sup>Shanghai Research Center for Quantum Science and CAS Center for Excellence in Quantum Information and Quantum Physics, University of Science and Technology of China, Shanghai 201315, China

<sup>6</sup>Hefei National Laboratory, University of Science and Technology of China, Hefei 230088, China

Quench experiments on a unitary Bose gas around a broad Feshbach resonance have led to the discovery of universal dynamics. This universality is manifested in the measured atomic momentum distributions where, asymptotically, a quasi-equilibrated metastable state is found in which both the momentum distribution and the time scales are determined by the particle density. In this paper we present counterpart studies but for the case of a very narrow Feshbach resonance of <sup>133</sup>Cs atoms having a width of 8.3 mG. In dramatic contrast to the behavior reported earlier, a rapid quench of an atomic condensate to unitarity is observed to ultimately lead to coherent oscillations involving dynamically produced condensed and non-condensed molecules and atoms. The same characteristic frequency, determined by the Feshbach coupling, is observed in all types of particles. To understand these quench dynamics and how these different particle species are created, we develop a beyond Hartree-Fock-Bogoliubov dynamical framework including a new type of cross correlation between atoms and molecules. This leads to a quantitative consistency with the measured frequency. Our results, which can be applied to the general class of bosonic superfluids associated with narrow Feshbach resonances, establish a new paradigm for universal dynamics dominated by quantum many-body interactions.

*Introduction.* Understanding the inherently unstable unitary Bose gas has remained a challenge [1–6]. Some progress, however, has been made principally because rapid field sweeps across a Feshbach resonance to unitarity show, fortuitously, that the gas lives long enough to reveal features of quasi-steady state behavior before inevitable losses set in. This is seen through the momentum distribution  $n(k)$  of non-condensed particles [7, 8]. Importantly, these sweeps establish that the signal at high momentum  $k$  grows and eventually saturates, as a function of time. These intriguing saturation phenomena have been referred to as a form of prethermalization [9, 10]. Interestingly, for the systems studied thus far, the time scale for such quasi-steady state dynamics is claimed to be universal. As the scattering length  $a_s \rightarrow \infty$ , it is presumed that time dependent phenomena should be determined by a single energy scale  $E_F \propto (6\pi^2 n)^{2/3}$  [11–16], where  $n$  is the density of bosons.

Here we emphasize that this form of universality does not apply to the narrow resonance case. Even at unitarity, the relevant energy scale corresponds to the many-body Feshbach coupling  $\alpha\sqrt{n}$ , which is to be contrasted with the Fermi energy  $E_F$ . This scale may be ignored in previous work [7, 8] since there  $\alpha\sqrt{n} \gg E_F$ . However, the dynamics of the unitary gas in this narrow resonance regime which has not received the same degree of attention, remains to be experimentally characterized and theoretically understood.

In this paper, using both theory and experiment, we investigate the case of this narrow Feshbach resonance. In contrast to previous Bose gas literature which focused on the atoms, one has access to a sizeable population of closed channel molecules which govern much of the physics at unitarity. Our

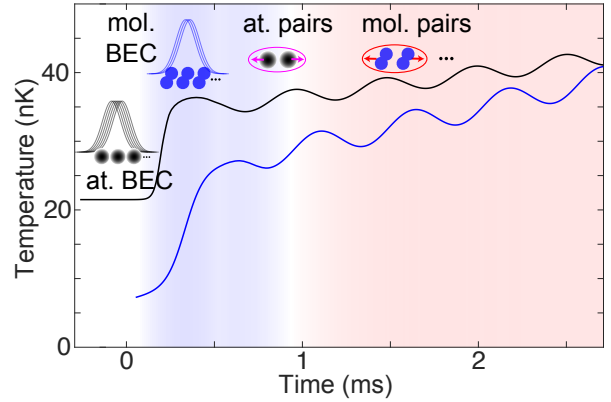


FIG. 1. Effective temperature of atoms (black solid line) and molecules (blue) based on an error-bar weighted fit to data from Ref.[17] emphasizing the creation of out-of-condensate particles deriving from an atomic BEC after a quench to unitarity, see Supplement [18]. The small cartoons indicate the different species of particles generated at different stages of the dynamics, including atomic and molecular BECs, finite-momentum atomic and molecular pairs.

work is motivated by an earlier observation of the effective temperature,  $T_{\text{eff}}$  of out-of-condensate atoms and of closed channel molecules [17] which is plotted in Fig. 1. These are created during a quench to unitarity of an atomic Bose-Einstein condensate (BEC) of <sup>133</sup>Cs atoms associated with a narrow resonance (of width 8.3 mG). Although previously oscillations in  $T_{\text{eff}}$  were not reported, they are revealed here based on an error-bar weighted fit to the temperature data.

It is our goal to experimentally investigate and theoretically

understand the initial creation and subsequent oscillatory dynamics of these excited atomic and molecular states. To this end, we employ a time-of-flight (TOF) procedure. By analyzing a data set from previous experiments [17, 19], we are able to characterize multiple new observables. These include the atomic and molecular particle number distribution at different momenta and their associated kinetic energies [18].

Theoretically to understand the oscillatory behavior observed in these quantities, we go beyond the Hartree-Fock-Bogolibov (HFB) [20, 21] approach and establish a new dynamical framework that includes atom-molecule correlations. These correlations, which have no counterpart in the broad resonance case, turn out to be central to the dynamics of the out-of-condensate particles. In the process we identify three distinct evolutionary stages in the quench dynamics; this is initiated by the generation of a molecular BEC and subsequently followed by the creation of finite-momentum atoms and molecules which then undergo coherent oscillations[17, 22]. Satisfactory quantitative agreement is obtained between theory and experiment both for the rather large oscillatory frequency which turns out to be around 2 kHz and for the net increase of kinetic energy (associated with the decay of the initial atomic condensate) which is transferred to newly excited atoms and molecules.

*Dynamical Framework.* The effective Hamiltonian for a magnetic Feshbach resonance is associated with coupling between atomic and molecular channels (respectively called “open” and “closed”). It is given by

$$\hat{H} = \sum_{\sigma} \int d^3x \hat{\psi}_{\sigma}^{\dagger}(x) \left( -\frac{\hbar^2 \nabla^2}{2m_{\sigma}} + \nu_{\sigma} \right) \hat{\psi}_{\sigma}(x) \quad (1)$$

$$+ \int d^3x \sum_{\sigma} \frac{g_{\sigma}}{2} \hat{\psi}_{\sigma}^{\dagger} \hat{\psi}_{\sigma}^{\dagger} \hat{\psi}_{\sigma} \hat{\psi}_{\sigma} - \left( \alpha \hat{\psi}_1^{\dagger} \hat{\psi}_1^{\dagger} \hat{\psi}_2 + h.c. \right).$$

Here  $\sigma = 1, 2$  represents the atoms and molecules, respectively, and  $\nu_{\sigma} = \delta_{\sigma,2}\nu$  where  $\nu$  is the detuning;  $g_{\sigma}$  is proportional to the background  $s$ -wave interaction, and  $\alpha$  corresponds to the important Feshbach coupling strength between the two channels. Model parameters are related to the physical quantities by  $g_{\sigma} = 4\pi\hbar^2 a_{\sigma}/(\Gamma_{\sigma} m_{\sigma})$ ,  $\alpha = \Gamma_1^{-1} \sqrt{2\pi\hbar^2 a_1 \delta\mu \Delta B}/m_1$  and  $\Gamma_{\sigma}$  is  $1 - 2a_{\sigma}\Lambda/\pi$  where  $\Lambda$  is a regularization cut-off. Here  $a_1$  and  $a_2$  are the background scattering length of atom and molecules,  $\delta\mu$  is the relative magnetic moment between open and closed channels and  $\Delta B$  is the resonance width. The detuning  $\nu$  is related to the physical detuning  $\nu_r = \delta\mu\delta B$  by  $\nu = \nu_r + \Lambda m_1 \Gamma_1 \alpha^2 / (\pi^2 \hbar^2)$  where  $\delta B$  is the distance of the magnetic field from the resonance. We use the experimental values [17] for the parameters  $a_1, a_2, \delta\mu, \Delta B$  and the initial atomic density  $n$  in the theoretical calculations [18].

To theoretically study non-equilibrium dynamics, we focus on one and two-point equal-time correlations as dynamical variables. This approach is related to others in the literature [23, 24] but now generalized to include the complexity of the two channel system. The one-point correlation  $\xi_{\sigma}(t) = V^{-1/2} \langle \hat{\psi}_{\sigma}(k=0, t) \rangle$  represents the atomic or

molecular condensate wavefunction, and  $c_{\sigma} \equiv |\xi_{\sigma}(t)|^2$  represents the condensate density. Operators representing the excitations are then given by  $\hat{\psi}'_{\sigma}(k) = \hat{\psi}_{\sigma}(k) - \delta_{k,0} \sqrt{V} \xi_{\sigma}(t)$ .

It is convenient to introduce a 4-vector field operator,  $\hat{\Psi}(k) = [\hat{\psi}'_1(k), \hat{\psi}'_1(-k), \hat{\psi}'_2(k), \hat{\psi}'_2(-k)]$ . The quantum fluctuations that involve the finite momentum particles correspond to two-point correlation functions,  $G_{\alpha\beta}(k) = \langle \hat{\Psi}_{\alpha}(-k) \hat{\Psi}_{\beta}(k) \rangle$ , from which we deduce physical quantities. The variables  $n_1(k) \equiv G_{21}(k)$  and  $n_2(k) \equiv G_{43}(k)$  represent the particle number associated with finite- $k$  atoms and molecules. Important are the interspecies correlations  $G_{13}(k)$  and  $G_{23}(k)$  which are central to the dynamics:  $G_{13}(k)$  is associated with the molecular pairs and  $G_{23}(k)$  controls the particle flow which results in the creation of finite- $k$  molecules.

The dynamical equations associated with these correlation functions are readily derived as

$$i\partial_t \xi_1 = 2g_1 n_1 \xi_1 + (g_1 \xi_1^2 + g_1 x_1 - 2\alpha \xi_2) \xi_1^* - 2\alpha f_{12}, \quad (2)$$

$$i\partial_t \xi_2 = (\nu + 2g_2 n_2) \xi_2 + (g_2 \xi_2^2 + g_2 x_2) \xi_2^* - \alpha(x_1 + \xi_1^2).$$

Here  $n_{\sigma} = \sum_{k \neq 0} n_{\sigma}(k)/V$  is the density of out-of-condensate atoms and molecules and  $V$  is the volume. We define  $x_1 = \sum_{k \neq 0} G_{11}(k)/V$  and  $x_2 = \sum_{k \neq 0} G_{33}(k)/V$  which represent atom and molecule pairs, respectively, as discussed in the supplement [18]. Additionally  $f_{12} = \sum_k G_{23}(k)/V$  characterizes the atom-molecule correlation function which plays an important role. The equations of motion for the 2-point correlations can be compactly written as

$$i\partial_t G_{mn}(k) = \sum_{\beta} L_{m\beta}(k) G_{\beta n}(k) + L_{n\beta}(k) G_{m\beta}(k) \quad (3)$$

where  $L(k)$  represents the coupling between finite-momentum atoms and molecules [18]. This dynamical scheme should be contrasted with the standard Hartree-Fock-Bogoliubov approach [20, 21] which omit these new atom-molecule correlations including  $f_{12}$ .

*Three Evolutionary Stages* Using these dynamical equations we identify different stages of particle creation throughout the quench dynamics. The quench of an atomic BEC to unitarity is implemented by an abrupt change in the detuning  $\nu_r \sim 0$  assuming initially, at  $t = 0$ , all particles reside in an atomic BEC. Fig. 2 indicates the three distinct dynamical stages where different species of particles are generated. In stage I, Feshbach couplings convert the initial atomic condensate into a coherent molecular BEC along with a small number of atomic and molecular pairs having momentum,  $\pm k$ . [25]. In stage II, shortly after its formation, the molecular BEC begins to partially decay and more atomic pairs appear. These latter in turn combine with an atom from the condensate to form an atom-molecule complex. The combination of an atom-molecule complex and an atom from the condensate is further converted into a pair of molecules. In stage III, with these finite-momentum atomic and molecular populations now fully formed, the system enters a stage of steady-state coherent oscillations.

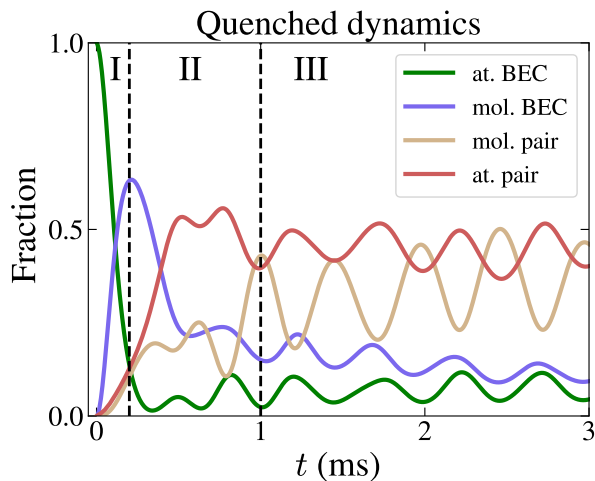


FIG. 2. Population transfers and growth in the present theory. When an atomic BEC is quenched to unitarity, a molecular BEC is the first to be created. After  $t = 0.2$  ms, both atomic and molecular BECs decay, generating a large fraction of non-condensed atoms and molecules. After 1 ms, all particles exhibit oscillations with identical frequency. Only the non-condensed molecules are out of phase as they control the flow of particles.

What is particularly interesting about these oscillations is that, at unitarity, there is an in-phase relationship between all quantities except for the non-condensed molecules. This phenomenon derives from a competition involving the three particle currents driven by the Feshbach coupling [18]. These currents represent the flow of particles between atoms and molecules and condensates. Our central finding is that at resonance, once non-condensed molecules are created, they tend to control (through the equations of motion) the general dynamics of the particles. As a consequence, the out-of-condensate molecules are, interestingly, out-of-phase with the other three species [18].

Most of the general observations we outline below (unless indicated otherwise) pertain to both theory and experiment [26] and these can be seen in Fig. 3. As is suggested by Figure 1, we find the newly generated out-of-condensate particles carry kinetic energy that also undergoes oscillatory dynamics. As the atomic condensate decays, a portion of the interaction energy is transferred to non-condensed particles as kinetic energy. This leads to an increase of the kinetic energy in both atoms and molecules right after the quench at  $t < 0.5$  ms. We can quantify this increase,  $E_K^\sigma/N_0$ , which is of the order of 10 nK for the atoms and 5 nK for the molecules, as found in both theory and experiment.

After this initial rise, the kinetic energy subsequently oscillates and these oscillations persist for a period of around 2 ms notably, without any sign of thermalization. This oscillatory frequency is around 2 kHz, which, importantly, coincides with that of the population oscillations (see Fig. 2) [17]. Indeed, this single oscillation pattern observed in all collective observables reflects the fact that the same underlying microscopic

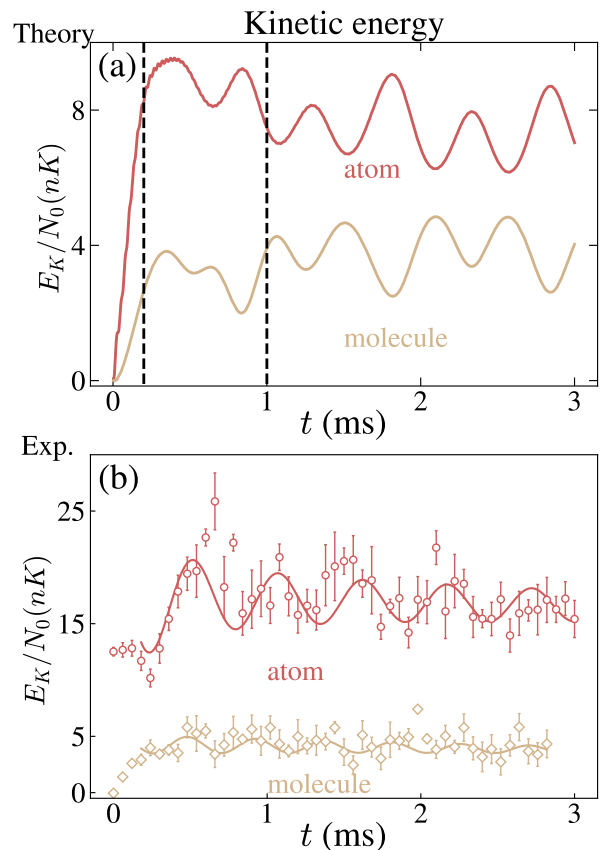


FIG. 3. Kinetic energy variation  $E_K/N_0$  for atoms and molecules which is associated with the population transfers and growth in Figure 2. Here  $E_K^\sigma/N_0 \equiv \int d^3k/(2\pi)^3 n_\sigma(k)(k_x^2 + k_y^2)/(2m_\sigma n)$ . Theory (top panel) and experiment (bottom panel). In experiment (but not theory) there is loss of particles which is associated with a gain in kinetic energy, but the two effects tend to at least partially compensate in the figure. Experiment and theory show similar oscillatory behavior and both show a net increase of kinetic energy which is of the order of 5 nK times  $N_0$ , where  $N_0$  represents the total number of particles at the start of the sweep.

dynamical processes are present.

*Momentum-resolved Distributions and Asymptotic Coherent Oscillations.* Of interest next is to clarify the microscopic mechanism responsible for the generation of finite-momentum particles, after the initial formation of the molecular BEC. This is associated with the Feshbach resonant interaction and is contained in the properties of the matrix  $L(k)$  in Eq. 3. The eigenvalues of  $L$  determine the speed of growth of these out-of-condensate particles while the eigenvectors determine the fraction of atoms and molecules involved in the generation process. We consider the eigenvalues of  $L(k)$ ,

$$\lambda_{\pm} \simeq \sqrt{F_1(k) \pm \sqrt{F_1^2(k) - 4F_2(k)}}. \quad (4)$$

Here  $F_1/F_2$  are given by  $F_1(k) = \epsilon_1^2(k) + \epsilon_2^2(k) + 8\alpha^2|\xi_1|^2 - 4\alpha^2|\xi_2|^2$  and  $F_2(k) = (\epsilon_1(k)\epsilon_2(k) - 4\alpha^2|\xi_1|^2)^2 - 4\alpha^2|\xi_2|^2\epsilon_2^2(k)$ . This depends on dispersions given by  $\epsilon_\sigma(k) =$

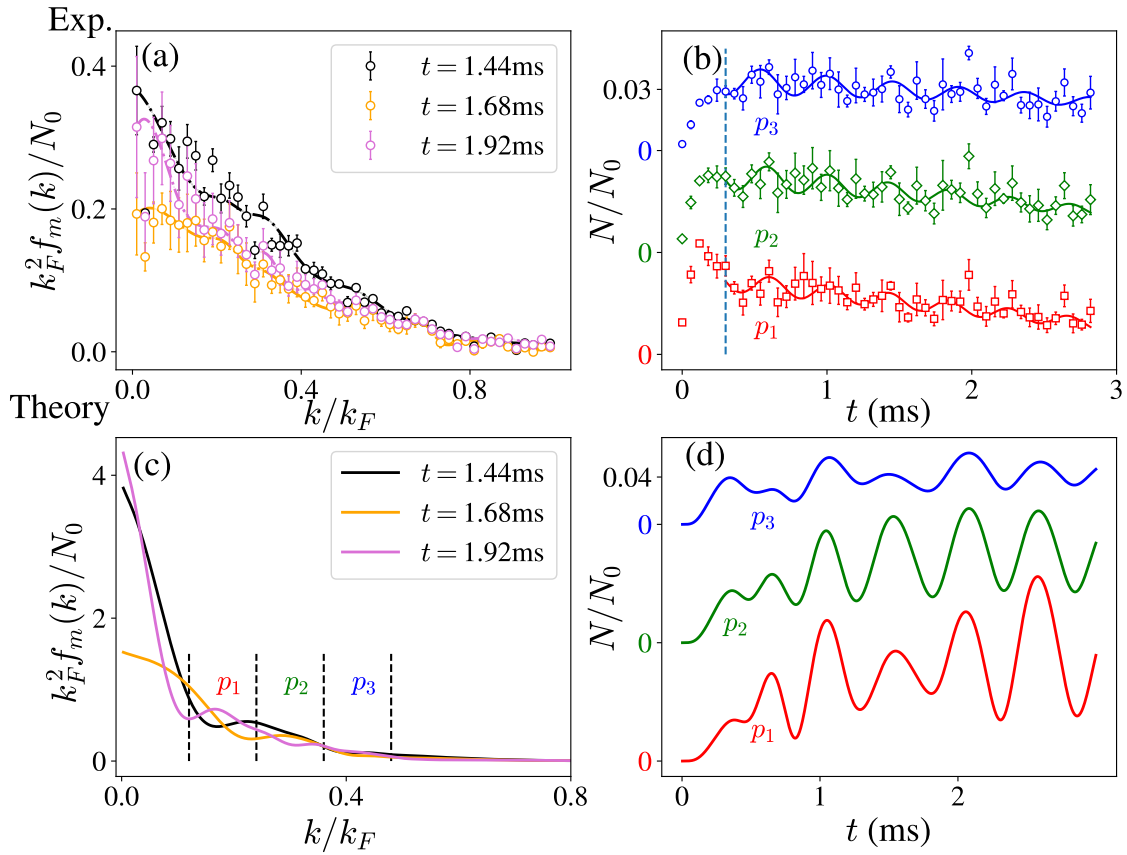


FIG. 4. Theory-experiment comparison of the dynamics of finite-momentum molecules where (a) represents experimentally measured momentum distribution  $f_m$  at 3 different times showing non-monotonicity—the ordering of the curves from top to bottom corresponds to early, then late and then middle time. Here  $f_m$  is the angular average momentum distribution of molecules such that  $\int d^2k f_m = N_m$ . (b) plots their number  $vs$  time,  $t$ , when summed over a momentum shell. The summation region is indicated by  $p_1/p_2/p_3$ . Here  $p_i = \int_{k_i \leq k < k_{i+1}} d^2k f_m(k)$  where  $k_i = 0.12k_F \times i$ . Panels (c) and (d) indicate the counterpart theory plots. We observe coherent oscillations in three different shells all with the same frequency of 2kHz in both theory and experiment. Comparing panels (a) and (c) suggests that the occupation of more and higher momentum states seen in experiment may reflect thermal effects: the experiments are performed at finite  $T$ , whereas theory is at  $T = 0$ .

$k^2/2m_\sigma + \nu_r \delta_{2,\sigma}$ . One may observe that there exist two circumstances which lead to an imaginary  $\lambda$  and a consequent instability of condensates: either  $F_1(k) < 0$  which is associated with the processes in stage I, or  $F_2(k) < 0$  which is mainly associated with those processes in stage II. These unstable outcomes are *unavoidable* when particles mostly reside in condensates. Indeed, once a molecular condensate is present ( $\xi_2 \neq 0$ ), one can always find a value of  $k$  such that  $\epsilon_1 \epsilon_2 - 4\alpha^2 |\xi_1|^2 \simeq 0$  leading to an imaginary value for  $\lambda_-$ . Additionally, for  $|\xi_2| \gg |\xi_1|$ , the instability occurs at  $\epsilon_1^2(k) + \epsilon_2^2(k) < 4\alpha^2 |\xi_2|^2$ . In this way, finite-momentum particles are exponentially generated.

All of this can be contrasted with the larger  $k$  regime where the eigenvalues are real and there is consequently no significant occupation of higher momentum states, say  $k$  of the order of  $k_F$ . Here the kinetic oscillations rather than the exponential growth dominates. Indeed, the momentum distributions we observe are consistent with the above analysis, where particles are seen to be concentrated in states with low momen-

tum up to  $\approx k_F/2$  where  $k_F \equiv (6\pi^2 n)^{1/3}$ . We stress that, in contrast to the saturation effects seen in the broad Feshbach resonance [7, 8], the momentum distributions in the narrow resonance case oscillate during the later time dynamics, as seen in Fig. 4a,c.

To confirm that a single oscillation frequency is present in the experiments, as suggested by theory, we determine the molecular population in a shell including different groupings of momenta  $p_i$ , as in Fig. 4. Three such subsets were considered and the behavior in all is found to be rather similar with all showing the characteristic frequency of 2 kHz. This shared common frequency between finite-momentum atoms and molecules and their condensates should be understood to derive from Feshbach coupling [18]. We note parenthetically that the amplitude of the oscillations is slightly greater in theory than experiment, which we attribute to finite temperature effects in our experiment that suppress the coherence of atoms and molecules.

A final challenge we must address is to understand the

microscopic origin of the ubiquitous 2kHz oscillation frequency. Notably, a frequency of this order is a large energy scale compared to other energy scales in the problem including, for example, the self-interaction energy terms deriving from  $g_1$  and  $g_2$  which are of the order of  $E_g/h \equiv g_{1/2}n \simeq 0.25\text{kHz}$ . To determine where this large frequency originates requires evaluating the separation of the energy levels between atomic and molecular condensates. We are able to identify the main contribution to this energy gap as coming from the new atom-molecule interspecies correlation  $f_{12}$ . This provides an additional self-energy correction to the atomic condensate  $\mu_1 = -2\alpha\text{Re} f_{12}/\xi_1$ , arising from the Feshbach coupling  $\sim \alpha\hat{\psi}_1^\dagger(x)\hat{\psi}_1^\dagger(x)\hat{\psi}_2(x)$  (see Eq. 3). Similarly, one finds the self-energy correction to the molecular condensate,  $\mu_2 = -\alpha\text{Re} x_1/\xi_2$ . They together determine the splitting of the atomic and molecular condensate levels:  $\Delta\mu = 2\mu_1 - \mu_2$ . It is notable that without this correction to  $\mu_1$ , the characteristic oscillation frequency would be around 0.9 kHz [19]. But with these corrections, we find that  $\Delta\mu$  is, indeed, around 2 kHz, bringing theory and experiment into reasonable agreement [18].

*Conclusion.* We have emphasized throughout that the coherent oscillations we observe for the narrow resonance case are universal as they are only determined by a *single* energy scale  $\alpha\sqrt{n}$ . This leads to a different paradigm for the universal dynamics of the unitary Bose gas. This is associated with a many body (Feshbach) coupling and is to be contrasted with the universality previously discussed in the literature [7, 8] and associated with the Fermi energy. As in this early literature, arriving at this universality requires us to focus on characterizing the dynamical behavior of non-condensed particles which appear when an atomic condensate is swept to unitarity. Here in addition to atoms there are out-of-condensate molecules, and once formed, all populations reach a steady oscillatory state; all finite-momentum particles are seen to have the same intrinsic oscillation frequency which is the same as that of the condensate [19].

In this context, we have presented a reasonably successful comparison between theory and experiment. Because of these quantitative correspondences we are able to glean support for a rather new and different dynamical theory. This is to be contrasted with the more conventional Hartree-Fock-Bogoliubov approach [20, 21]. Importantly, this dynamical machinery and its rich phenomenology should be relevant to the general class of bosonic superfluids associated with narrow Feshbach resonances.

*Acknowledgement* This work is supported by the National Science Foundation under Grant No. PHY1511696 and PHY-2103542, and by the Air Force Office of Scientific Research under award number FA9550-21-1-0447. We thank Cheng Chin for helpful discussions. Z.Z. acknowledges the Bloch Postdoctoral Fellowship. S.N. acknowledges support from the Takenaka Scholarship Foundation. Z.W. is supported by the Innovation Program for Quantum Science and Technology (Grant No. 2021ZD0301904). We also acknowledge the

University of Chicago’s Research Computing Center for their support of this work.

- 
- [1] S. B. Papp, J. M. Pino, R. J. Wild, S. Ronen, C. E. Wieman, D. S. Jin, and E. A. Cornell, Phys. Rev. Lett. **101**, 135301 (2008).
  - [2] N. Navon, S. Piatecki, K. Günter, B. Rem, T. C. Nguyen, F. Chevy, W. Krauth, and C. Salomon, Phys. Rev. Lett. **107**, 135301 (2011).
  - [3] S. E. Pollack, D. Dries, M. Junker, Y. P. Chen, T. A. Corcovilos, and R. G. Hulet, Phys. Rev. Lett. **102**, 090402 (2009).
  - [4] S. Piatecki and W. Krauth, Nature Communications **5**, 3503 (2014).
  - [5] R. J. Wild, P. Makotyn, J. M. Pino, E. A. Cornell, and D. S. Jin, Phys. Rev. Lett. **108**, 145305 (2012).
  - [6] E. Braaten, D. Kang, and L. Platter, Phys. Rev. Lett. **106**, 153005 (2011).
  - [7] P. Makotyn, C. E. Klauss, D. L. Goldberger, E. A. Cornell, and D. S. Jin, Nature Physics **10**, 116 (2014).
  - [8] C. Eigen, J. A. P. Glidden, R. Lopes, E. A. Cornell, R. P. Smith, and Z. Hadzibabic, Nature **563**, 221 (2018).
  - [9] X. Yin and L. Radzihovsky, Phys. Rev. A **94**, 039901 (2016).
  - [10] A. Rançon and K. Levin, Phys. Rev. A **90**, 021602 (2014).
  - [11] S. Cowell, H. Heiselberg, I. E. Mazets, J. Morales, V. R. Pandharipande, and C. J. Pethick, Phys. Rev. Lett. **88**, 210403 (2002).
  - [12] J. L. Song and F. Zhou, Phys. Rev. Lett. **103**, 025302 (2009).
  - [13] Y.-L. Lee and Y.-W. Lee, Phys. Rev. A **81**, 063613 (2010).
  - [14] J. M. Diederix, T. C. F. van Heijst, and H. T. C. Stoof, Phys. Rev. A **84**, 033618 (2011).
  - [15] W. Li and T.-L. Ho, Phys. Rev. Lett. **108**, 195301 (2012).
  - [16] S.-J. Jiang, W.-M. Liu, G. W. Semenoff, and F. Zhou, Phys. Rev. A **89**, 033614 (2014).
  - [17] Z. Zhang, S. Nagata, K.-X. Yao, and C. Chin, Nature Physics **19**, 1466 (2023).
  - [18] See supplementary materials.
  - [19] Z. Wang, K. Wang, Z. Zhang, S. Nagata, C. Chin, and K. Levin, Phys. Rev. A **110**, 013306 (2024).
  - [20] S. Kokkelmans and M. Holland, Physical Review Letters **89**, 180401 (2002).
  - [21] V. Snyder, S. Kokkelmans, and L. D. Carr, Physical Review A—Atomic, Molecular, and Optical Physics **85**, 033616 (2012).
  - [22] Y. Tian, Y. Zhao, Y. Wu, J. Ye, S. Mei, Z. Chi, T. Tian, C. Wang, Z.-Y. Shi, Y. Chen, J. Hu, H. Zhai, and W. Chen, “Dissipation driven coherent dynamics observed in bose-einstein condensates,” (2024), arXiv:2408.03815 [cond-mat.quant-gas].
  - [23] V. E. Colussi, H. Kurkjian, M. Van Regemortel, S. Musolino, J. van de Kraats, M. Wouters, and S. J. J. M. F. Kokkelmans, Phys. Rev. A **102**, 063314 (2020).
  - [24] M. Van Regemortel, H. Kurkjian, M. Wouters, and I. Carusotto, Phys. Rev. A **98**, 053612 (2018).
  - [25] The growth of this molecular BEC is associated with instanton dynamics:  $\xi_2(t)/\sqrt{n} = i \tanh(t/t_\alpha)$ , where  $t_\alpha = \hbar/\alpha\sqrt{2n}$  [18].
  - [26] Because the experimentally observed particle loss is not significant within the 3 ms time frame [17], it makes sense to consider these comparisons.

# Supplemental Material for Dynamics of the unitary Bose gas near a narrow Feshbach resonance: universal coherent atom-molecule oscillations

Ke Wang,<sup>1,2</sup> Zhendong Zhang,<sup>3</sup> Shu Nagata,<sup>1</sup> Zhiqiang Wang,<sup>1,4,5,6</sup> and K. Levin<sup>1</sup>

<sup>1</sup>*Department of Physics and James Franck Institute, University of Chicago, Chicago, Illinois 60637, USA*

<sup>2</sup>*Kadanoff Center for Theoretical Physics, University of Chicago, Chicago, Illinois 60637, USA*

<sup>3</sup>*E. L. Ginzton Laboratory and Department of Applied Physics, Stanford University, Stanford, CA 94305, USA*

<sup>4</sup>*Hefei National Research Center for Physical Sciences at the Microscale and School of Physical Sciences, University of Science and Technology of China, Hefei, Anhui 230026, China*

<sup>5</sup>*Shanghai Research Center for Quantum Science and CAS Center for Excellence in Quantum Information and Quantum Physics, University of Science and Technology of China, Shanghai 201315, China*

<sup>6</sup>*Hefei National Laboratory, University of Science and Technology of China, Hefei 230088, China*

## S1. EXPERIMENTAL BACKGROUND

### A. Typical experimental parameters and characterization of the momentum distribution

For <sup>133</sup>Cs the resonance at  $B = 19.849$  G has a very small width of  $\Delta = 8.3$  mG : the experimental parameters are given by  $\delta\mu = 2\pi\hbar \times 0.76$  MHz/G,  $a_{\text{bg}} = 163a_0$  where  $a_0$  is Bohr radius. The molecular  $s$ -wave scattering length is  $a_2 = 220a_0$ . The mean BEC density is  $n = 3 \times 10^{13}$  cm<sup>-3</sup>.

We extract experimentally from time of flight (TOF) measurements the particle number density distribution in a two-dimensional space given by  $n_{a/m}^{\text{TOF}}(x, y)$  which represents the atom and molecule particle number per pixel. Relating momentum and position variables  $\hbar\mathbf{k} = m\omega\mathbf{x}$ , we find that

$$\mathbf{k}_a = 0.193(\mu m^{-2}) \times \mathbf{x}_a, \quad \mathbf{k}_m = 0.387(\mu m^{-2}) \times \mathbf{x}_m. \quad (\text{S1})$$

Here  $\mathbf{k}_{a/m}$  represents the momentum of atoms or molecules while  $\mathbf{x}_{a/m}$  represents their positions. In this way one can use Eq. S1 to obtain a particle number distribution in momentum space,

$$N_{a/m}(k_x, k_y, t) = n_{a/m}^{\text{TOF}}(x, y, t) \times S_{\text{pixel}} = n_{a/m}^{\text{TOF}}(x, y, t) \times (0.605\mu m)^2 \quad (\text{S2})$$

Here we use the area of a single pixel  $S_{\text{pixel}} = 0.605^2\mu m^2$ . The mean BEC density is  $n = 3 \times 10^{13}$  cm<sup>-3</sup>, which defines a momentum scale,

$$k_F = (6\pi^2 n)^{1/3} \simeq 12.1\mu m^{-1}. \quad (\text{S3})$$

To visualize the 2D data as a 1D curve, we perform the angular average below to obtain a momentum distribution,

$$f_{a/m}(k_i, t) := \frac{1}{2\pi(k_i + \Delta/2)\Delta} \sum_{k_i \leq \sqrt{k_x^2 + k_y^2} < k_i + \Delta} N_{a/m}(k_x, k_y, t), \quad k_i = i\Delta. \quad (\text{S4})$$

Here  $f$  has the dimensions of area and  $\Delta = k_F/50$ . This allows us to obtain the momentum distribution as given in the main-text with the normalization

$$\int d^2k f_{a/m}(k, t) = N_{a/m} \quad (\text{S5})$$

### B. Alternative fit of the effective temperature data in Ref. [17].

In contrast to an earlier empirical fit to the effective temperature, in Fig 1 we use a sinusoidal function plus a linear increasing offset  $y(t) = A \sin(2\pi ft + \phi) + Bt + C$  to fit the coefficients (A,B,C) based on the error bars in the data. In this way we can replot the atomic and molecular temperature data presented in Fig.3b of Ref. [17]. We choose to fit the data points at  $t > 0.5$  ms when they start to oscillate. The oscillation frequencies are determined to be 2.0(2) kHz for atoms and 1.9(2) kHz for molecules, which are consistent with the universal 2 kHz oscillation frequency seen in other observables shown in the main text.

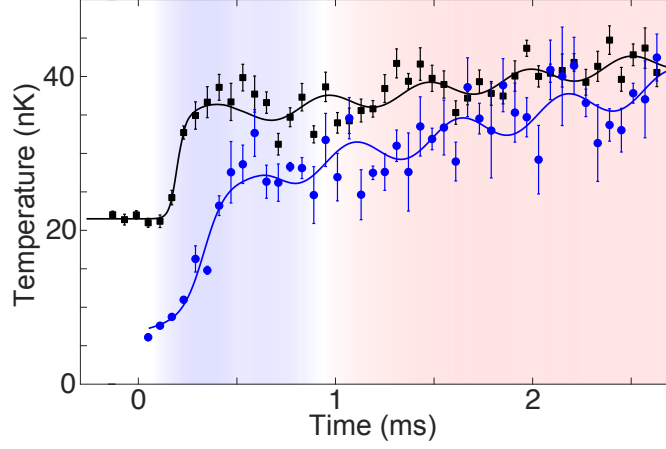


FIG. S1. Effective temperature of atoms (black points) and molecules (blue points) from Ref. [17]. Data points at  $t > 0.5$  ms are fit using the function  $y(t) = A \sin(2\pi ft + \phi) + Bt + C$ . The fit determines the oscillation frequency  $f$  to be 2.0(2) kHz for atoms and 1.9(2) kHz for molecules. The parts of the curves at  $t \leq 0.5$  ms are guides to the eye.

## S2. THEORETICAL ANALYSIS

### A. Two-dimensional momentum distribution

We theoretically compute the particle number distribution in momentum space,  $n(k)$ . When integrated over momentum this yields the density in each channel,  $n = \int \frac{d^3k}{(2\pi)^3} n(k)$ . Of interest is the integral along the  $z$ -axis representing a column integrated two dimensional distribution. We define

$$F_{a/m}(k_{\perp}) = \int \frac{dk_z}{2\pi} n_{a/m} \left( \sqrt{k_{\perp}^2 + k_z^2} \right) \quad (\text{S6})$$

Imposing a normalization condition  $(2\pi)^{-2} \int d^2k_{\perp} F_{a/m} = N_{a/m}/V$  yields the following relation between  $F_{a/m}$  and the variable  $f_{a/m}$ ,

$$\frac{V}{(2\pi)^2} F_{a/m}(k) = f_{a/m}(k) \iff \frac{N_0/n}{(2\pi)^2} F_{a/m}(k) = f_{a/m}(k), \quad (\text{S7})$$

which allows us to relate the theory to experimental data  $f_{a/m}$ . Here  $N_0$  is the initial particle number. The dimensionless quantity plot in Fig. 3c of the main-text is based on the relation:

$$\frac{k_F^2 f_{a/m}}{N_0} = (2\pi)^2 \frac{k_F^2}{n} F_{a/m}(k). \quad (\text{S8})$$

### B. Derivation of the Dynamical Equations

In this section, we discuss the 2-channel model and the associated dynamical equations. We start from the effective field theory of the Hamiltonian

$$H = \sum_{\sigma} \int d^d x \hat{\psi}_{\sigma}^{\dagger}(x) \left( -\frac{\nabla^2}{2m_{\sigma}} + \nu_{\sigma} \right) \hat{\psi}_{\sigma}(x) + \int d^d x \left( \sum_{\sigma} \frac{g_{\sigma}}{2} |\hat{\psi}_{\sigma}(x)|^4 - \alpha \hat{\psi}_1^{\dagger}(x) \hat{\psi}_1^{\dagger}(x) \hat{\psi}_2(x) - h.c. \right). \quad (\text{S9})$$

Here  $\sigma = 1, 2$  refers to the open channel atoms and closed-channel molecules,  $g_{\sigma}$  represents the background  $s$ -wave interaction in the open and closed channels and  $\alpha$  represents the Feshbach coupling strength between two channels. Here  $\nu_1 = 0$  and  $\nu_2 - \nu_1$  is related to the binding energy of molecules. This model allows us to address the kinematics of the open channel atoms and closed channel molecules, and the couplings between them. We note that with the appropriate parameters we are able to reproduce the resonance width and the 2-body scattering length of atoms.

To address the quantum dynamics we relate the fundamental dynamical variables in our model to the equal-time correlation functions of field operators. Here the one-point correlation function represents the condensate wave-function,

$$\xi_\sigma = \frac{1}{\sqrt{V}} \langle \hat{\psi}_\sigma(k=0) \rangle, \quad \sigma = 1, 2. \quad (\text{S10})$$

With this definition we deduce the *exact* equation of motion for condensates,

$$\begin{aligned} i \frac{d}{dt} \xi_1 &= 2g_1 n_1 \xi_1 + (g_1 x'_1 - 2\alpha \xi_2) \xi_1^* - 2\alpha f_{12} + g_1 f_{111} \\ i \frac{d}{dt} \xi_2 &= (\nu + 2g_2 n_2) \xi_2 + g_2 x'_2 \xi_2^* - 2\alpha x'_1 + g_2 f_{222} \end{aligned} \quad (\text{S11})$$

where we denote

$$f_{12} = \int d^3 q / (2\pi)^3 \langle \psi_1^\dagger(q) \psi_2'(q) \rangle, \quad f_{\sigma\sigma\sigma} = \int d^3 q_1 d^3 q_2 / (2\pi)^6 \langle \psi_\sigma^\dagger(q_1) \hat{\psi}'_\sigma(q_2) \hat{\psi}'_\sigma(q_1 - q_2) \rangle. \quad (\text{S12})$$

$$n_\sigma = \int d^3 q / (2\pi)^3 \langle \psi_\sigma^\dagger(q) \psi'_\sigma(q) \rangle, \quad x'_\sigma = \xi_\sigma^2 + \int d^3 q / (2\pi)^3 \langle \psi'_\sigma(q) \psi'_\sigma(-q) \rangle. \quad (\text{S13})$$

Here  $n_\sigma$  represents the number of particles in finite momentum states.

The correlation functions are given in terms of  $\hat{\psi}'_\sigma(k) = \hat{\psi}_\sigma(k) - \delta_{k,0} \xi_\sigma$  where we have introduced a 4-vector field operator,  $\Psi = (\psi'_1, \psi_1^\dagger, \psi'_2, \psi_2^\dagger)$ . One may define a general  $n$ -point correlation function below,

$$G_{i_1, i_2, \dots, i_n}(k_1, k_2, \dots, k_n) = \langle \hat{\Psi}_{i_1}(k_1) \hat{\Psi}_{i_2}(k_2) \dots \hat{\Psi}_{i_n}(k_n) \rangle. \quad (\text{S14})$$

Next we derive the dynamics of these correlation functions using the time evolution operator,  $\hat{U}(t) = \exp(-i\hat{H}t)$  based on the Hamiltonian in Eq. S9. This yields the following equations of motion:

$$i \frac{d}{dt} \hat{\Psi}_i(k) = L'_{i\beta}(k) \hat{\Psi}_\beta(k) + \sum_q Q_{i\beta\gamma} \hat{\Psi}_\beta(q) \hat{\Psi}_\gamma(k-q) + \sum_{q_1, q_2} C_{i\beta\gamma\delta} \hat{\Psi}_\beta(q_1) \hat{\Psi}_\gamma(q_2) \hat{\Psi}_\delta(k-q_1-q_2).$$

Here  $L'$  is 2 point vertex related to the quadratic part of Hamiltonian,  $Q$  is the 3-point vertex which includes the Feshbach coupling term while  $C$  is a 4-point vertex including background scatterings. Only a few values of  $Q_{\alpha\beta\gamma}$  are non-vanishing. These are given by

$$\begin{aligned} Q_{121} &= \frac{2g_1 \xi_1}{\sqrt{V}}, \quad Q_{111} = \frac{g_1 \xi_1^*}{\sqrt{V}}, \quad Q_{123} = -\frac{2\alpha}{\sqrt{V}}; \quad Q_{221} = -\frac{2g_1 \xi_1^*}{\sqrt{V}}, \quad Q_{222} = -\frac{g_1 \xi_1^*}{\sqrt{V}}, \quad Q_{214} = \frac{2\alpha}{\sqrt{V}}; \\ Q_{343} &= \frac{2g_2 \xi_2}{\sqrt{V}}, \quad Q_{333} = \frac{g_2 \xi_2^*}{\sqrt{V}}, \quad Q_{311} = -\frac{\alpha}{\sqrt{V}}; \quad Q_{443} = -\frac{2g_2 \xi_2^*}{\sqrt{V}}, \quad Q_{444} = -\frac{g_2 \xi_2^*}{\sqrt{V}}, \quad Q_{422} = \frac{\alpha}{\sqrt{V}}; \end{aligned} \quad (\text{S15})$$

Similarly, only a few values for  $C$  are non-zero,

$$C_{1211} = \frac{g_1}{V}, \quad C_{2221} = -\frac{g_1}{V}, \quad C_{3433} = \frac{g_2}{V}, \quad C_{4443} = -\frac{g_2}{V}. \quad (\text{S16})$$

This leads to the following heirarchy of equations,

$$\begin{aligned} i \frac{d}{dt} G_{i_1, i_2, \dots, i_n}(k_1, \dots, k_n) &= \sum_{j, \beta} L_{i_j \beta}(k_j) G_{i_1, \dots, i_{j-1}, \beta, i_{j+1}, \dots, i_n}(k_1, \dots, k_n) \\ &+ \sum_{j, \beta \gamma} Q_{i_j \beta \gamma} \sum_q G_{i_1, \dots, i_{j-1}, \beta, \gamma, i_{j+1}, \dots, i_n}(k_1, \dots, k_{j-1}, q, k_j - q, k_{j+1}, \dots, k_n) \\ &+ \sum_{j, \beta \gamma \delta} C_{i_j \beta \gamma \delta} \sum_{q_1, q_2} G_{i_1, \dots, i_{j-1}, \beta, \gamma, \delta, i_{j+1}, \dots, i_n}(k_1, \dots, k_{j-1}, q_1, q_2, k_j - q_1 - q_2, k_{j+1}, \dots, k_n) \end{aligned} \quad (\text{S17})$$

which relates  $n$ -point correlations with  $n(L)$ ,  $n+1(Q)$ ,  $n+2(C)$  correlations.

Now consider a quench of a pure atomic condensate to unitarity. It is useful to consider the way in which the dynamics reflects a sequence of *propagation of information* in the correlation functions,

$$\xi_1 \longrightarrow \xi_2 \longrightarrow G_{\alpha\beta} \longrightarrow G_{\alpha\beta\gamma} \longrightarrow \dots \quad (\text{S18})$$



Correspondingly, we can consider a sequence of points on the time axis,

$$t = 0 \longrightarrow t_1 \longrightarrow t_2 \longrightarrow t_3 \longrightarrow \dots \quad (\text{S19})$$

Because of the small size of the coupling constant  $\alpha$ , one may have well-separated dynamical regimes

$$\text{I} = [0, t_1], \text{II} = [t_1, t_2], \text{III} = [t_2, t_3], \dots \quad (\text{S20})$$

We stress here the importance of the subscript  $i$  in this discussion. The  $i$  associated with  $t_i$  indicates the time interval where the  $i$ -point correlation is fully developed and becomes non-perturbative. For example, in the time interval associated with  $t_2$  we need only include 2-point correlation functions in modeling the dynamics.

We observe that with increasing time the atomic and molecular BEC's decay and the coherence of the dynamical system is significantly reduced after the time frame  $t_2$ . Since the coherence greatly enhances the speed of reaction/collision events, we expect that the time scale of each stage monotonically increases such that  $t_3 - t_2 \gg t_2 - t_1 \gg t_1$ . Therefore the time required to fully develop the 3-point correlation is much longer than the  $t_2$ , which is the order of 1ms. Within the experimentally accessible time scale ( $< 3\text{ms}$ ), one may conclude that the contribution of 3-point correlation to the dynamics is subleading compared to the 2-point correlation. As a consequence in modeling the dynamics we set 3-point correlations to be zero and decompose 4-point correlations into products of 2-point correlation functions. Note that 3-point correlations are indecomposable since the average of  $\psi'$  is zero by definition. This then leads to a closed form for the dynamical equations (now consisting of only one-point and two-point functions.)

Within this approximation, one can derive an expression for the dynamical matrix,  $L$ , which appears in Eq. 3 of the main text,

$$L = \begin{pmatrix} \epsilon_1(k) & g_1 x'_1 - 2\alpha \xi_2 & -2\alpha \xi_1^* & 0 \\ -(g_1 x'_1 - 2\alpha \xi_2)^* & -\epsilon_1(-k) & 0 & 2\alpha \xi_1 \\ -2\alpha \xi_1 & 0 & \epsilon_2(k) & g_2 x'_2 \\ 0 & 2\alpha \xi_1^* & -g_2 x'_2 & -\epsilon_2(-k) \end{pmatrix} \quad (\text{S21})$$

where  $\epsilon_i(k) = k^2/2m_i + \nu_r \delta_{2,i} + 2g_i n_i$ .

### C. Different stages in the dynamical evolution

After the quench of the atomic BEC, the next most immediate stage of the dynamical evolution involves the creation of a molecular condensate. To describe this we begin by considering the dynamics with only two condensates,  $\xi_1$  and  $\xi_2$ . We set  $g_1 = g_2 = 0$  for simplicity. Since our focus is on unitarity, we set the detuning to zero. This leads to the coupled equations below,

$$i\partial_t \xi_1 = -2\alpha \xi_2 \xi_1^*, \quad i\partial_t \xi_2 = -\alpha \xi_1^2. \quad (\text{S22})$$

One may use the constraint from the conservation of particle-number  $|\xi_1|^2 + 2|\xi_2|^2 = n$  to eliminate  $\xi_1$  and find a single equation for  $\xi_2$ ,

$$\partial_t^2 \xi_2 + 4\alpha^2 \xi_2 (n - |\xi_2|^2) = 0. \quad (\text{S23})$$

With the initial condition from the quenched dynamics  $\xi_2(0) = 0$ ,  $\partial_t \xi_2(0) = i\alpha n$ , the differential equation allows an instanton solution,

$$\xi_2 = i\sqrt{n} \tanh\left(\alpha\sqrt{2nt}\right). \quad (\text{S24})$$

This in turn sets a time scale for the growth of the molecular condensate,  $t_\alpha = \hbar/\alpha\sqrt{n}$ . Due to the narrow Feshbach resonance, this time is not particularly small and the time scale should be observable in experiment as it is of the order of 0.2ms. Such instanton phenomena are characterized by a sharp peak in the particle fraction of the molecular BEC as a function of time which can be seen in Fig. 2 of the maintext.

### D. Determining the Oscillation Frequency

In the main text, we note that a gap is dynamically generated between the atomic and molecular BEC. This gap originates from the energy level difference  $\Delta\mu = 2\Delta\mu_1 - \Delta\mu_2$  between the two condensates. Here,  $\Delta\mu_\sigma$  represents the self-energy correction in this non-equilibrium setup[? ]:

$$\Delta\mu_1 = -2\alpha \text{Re} \xi_1^{-1} \sum_k \langle \psi_1^\dagger(k) \psi_2(k) \rangle, \quad \Delta\mu_2 = -\alpha \text{Re} \xi_2^{-1} \sum_k \langle \psi_1(k) \psi_1(-k) \rangle. \quad (\text{S25})$$

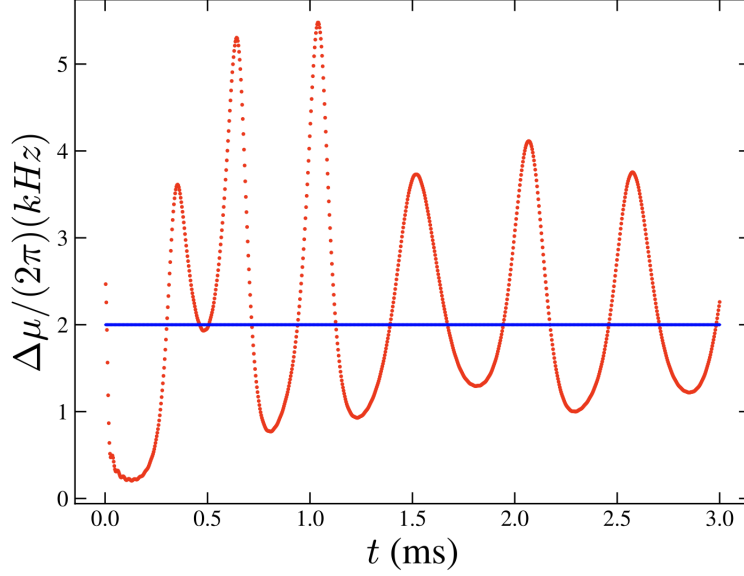


FIG. S2. The figure plots  $\Delta\mu$  as the function of time. Here  $h = 1$ . Numerically we find that the average of  $\Delta\mu$  in the late time is around 2.1kHz.

These functions  $\Delta\mu$  are time-dependent and oscillate around a constant value. The physical energy gap should be determined by the time-average  $\langle \Delta\mu \rangle_t$ ; see Fig. S2.

The finite momentum particles will also oscillate at the same frequency as the condensates. Because they have a generally kinetic energy,  $\epsilon_k/h \ll 2\text{kHz}$ , this will not appreciably alter the characteristic frequency.

### E. Coherent Particle Flow Currents

There are four species of particles in the system. Let us denote them by

$$c_1, c_2 : \text{This labels the particles in the atomic and molecular BECs,} \quad (\text{S26})$$

$$n_1, n_2 : \text{This labels the finite momentum particles for atoms or molecules.} \quad (\text{S27})$$

Particles flow among all four species as plotted in Fig. S3. The equations governing the dynamics (and counted in terms of the number of atoms) are:

$$\frac{d}{dt}c_1 = -J_1 - J_2, \quad \frac{d}{dt}c_2 = J_1/2 - J_3, \quad \frac{d}{dt}n_1 = -J_2 + 2J_3, \quad \frac{d}{dt}n_2 = J_2. \quad (\text{S28})$$

The currents are controlled by the phases of condensates and of the various finite-momentum correlation functions. This leads to expressions for the various currents:

$$J_1 = 4\alpha c_1 \sqrt{c_2} \sin(\phi_2 - 2\phi_1), \quad J_2 = 4\alpha |f_{12}| \sqrt{c_2} \sin(\theta_f - \phi_1), \quad J_3 = 2\alpha |x_1| \sqrt{c_2} \sin(\theta_x - \phi_2). \quad (\text{S29})$$

Here  $\phi_1$  and  $\phi_2$  are phases of atomic and molecular condensates, and  $\theta_f$  and  $\theta_x$  are phases of the complex numbers  $f_{12}$  and  $x_1$ .

All finite momentum particles collectively determine these two phases. The net particle flow results from a competition between these three different current which mostly consist of low  $k$  states. At resonance, we find that  $|J_2| > |J_1| > 2|J_3|$  and that  $J_2$  has a different sign from  $J_1$  and  $J_3$  at least after 1ms. It then follows that the out-of-condensate molecules (represented by  $n_2$ ) are out-of-phase with the other three species of particles.

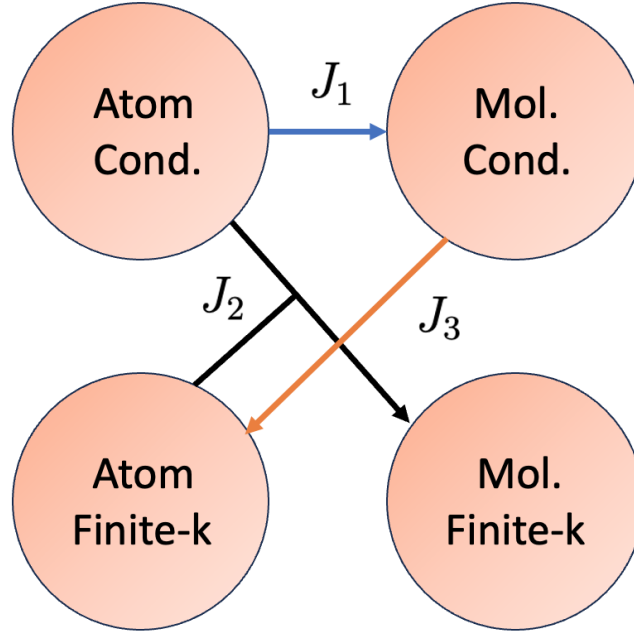


FIG. S3. There are three types of currents flow. (1)  $J_1$ : two cond. atoms form a molecule. (2)  $J_2$ : One cond. atom combine with one finite- $k$  atom, forming a finite momentum molecule. (3)  $J_3$ . One cond. Molecule dissociate into two finite- $k$  atoms.

#### F. The generation of Atom-molecule complexes and molecule-molecule pairs

In this section, we expand the discussion surrounding Eq. 3 in the main-text to illustrate how the atomic and molecular pairs are generated through the 2-point correlation functions involving the Feshbach coupling,

$$\begin{aligned}
 i\partial_t n_1(k) &= -2\alpha \left( f_{12}(k)\xi_1^\dagger + x_1^*(k)\xi_2 - h.c. \right), & i\partial_t n_2(k) &= -2\alpha \left( f_{12}^*(k)\xi_1 - h.c. \right), \\
 \left( i\partial_t + \frac{k^2}{m} \right) x_1(k) &= -2\alpha \left( 2a_{12}(k)\xi_1^\dagger + (2n_1(k) + 1)\xi_2 \right), & \left( i\partial_t + \frac{k^2}{2m} \right) x_2(k) &= -2\alpha \left( a_{21}(k)\xi_1 + \xi_1 a_{12}(k) \right). \\
 \left( i\partial_t + \frac{3k^2}{4m} - \nu \right) a_{12}(k) &= -2\alpha \left( x_2(k)\xi_1^\dagger + \xi_2 f_{12}(k) + x_1(k)\xi_1 \right), & \left( i\partial_t - \frac{k^2}{4m} - \nu \right) f_{12}(k) &= -2\alpha \left( n_1(k)\xi_1 - n_2(k)\xi_1 - a_{12}(k)\xi_2^\dagger \right).
 \end{aligned}$$

Here  $a_{12}(k) = \langle \psi_1'(k)\psi_2'(-k) \rangle = a_{21}(-k)$ . In a more concrete example, assume that one starts from a molecular condensate, and considers the simultaneous dissociation of an molecular condensate ( $\xi_2$ ) into atom pairs ( $x_1$ ). Then this pair of atoms can combine with an atom to form an atom-molecule complex, ( $a_{12}$ ), which can then combine with an atom and further generate a molecule pair ( $x_2$ ).